

DETECTORS SENSING SECOND SOUND EVENTS INDUCED BY THERMAL QUENCHES OF SRF CAVITIES IN HE II

M. Fouaidy, D. Longuevergne, F. Dubois, O. Pochon, J-F Yaniche, Institut de Physique Nucléaire d'Orsay Unité mixte de recherche CNRS-IN2P3 Université Paris-Sud 91406 ORSAY cedex

Abstract

SRF bulk Nb cavities are often limited by quench due to anomalous losses (Joule heating due normal defects or Field Emission). We continued R&D on Quench Detectors (QD) activity for locating quench in SRF cavities via 2nd sound in superfluid helium. We investigated 2 kinds of QD: Capacitive OST (COST) and Low Response time resistive Thermometers (LRT). A test stand operating in LHe (Temperature: T_0) was used for full characterization of the QD by means of precise experimental simulation of SRF cavity quench: various heaters subjected to a pulsed heat flux q_p were used. For improving spatial resolution of QD, smaller COSTs were developed and tested. We investigated the dynamic response of QD as function of different parameters (heater size/geometry, T_0 , q_p) and data are reported. Further, a 2nd Sound Resonator (SSR) equipped with a pair of COSTs at its 2 extremities as 2nd Sound Generator (SSG) and Detector (SSD) respectively, a low heat capacity heater (SSG) and a LRT (SSD) was developed. The experimental data obtained, with SSR operated in resonating mode or in a pulsed mode are presented. The results concerning location of quenches in QWR and Double-spoke cavities are discussed.

INTRODUCTION

Thanks to an important R&D effort made by different laboratories around the world during ~35 years, to the use of high purity material (e.g. Nb with RRR>300) and the improvement of fabrication process as well as preparation procedures, SRF bulk Nb cavities are nowadays operated reliably at high accelerating gradient E_{acc} . For example, in the frame ILC R&D program, the achieved E_{acc} in the TTF/FLASH superconducting linac at DESY increased from 18 MV/m for the 1st cryomodules housing 8 nine cells 1.3 GHz cavities to 30 MV/m for the 7th cryomodules. These 2 values of E_{acc} correspond to surface magnetic fields $B_S = 76$ mT and 126 mT respectively [1]. However, the maximum RF surface magnetic field (B_{Smax}) achieved with SRF bulk Nb cavities is often limited by anomalous RF losses due to Joule heating of normal-resistive defects embedded onto the RF surface or heating induced by impacting field emitted electrons on the RF surface. The typical effective diameter and surface resistance of normal defects are respectively in the range 1-100 μm and 1-10 m Ω . Considering a ILC cavity operating at $E_{acc}=33$ MV/m, the heat flux density q_{Defect} due to Joule heating of a defect area is 31 MW/m² (Fig.1), in contrast to RF losses in the superconducting RF surface region ($q_{BCS}\sim 82$ W/m²). Due to such very high heat flux in the defect zone, and to the

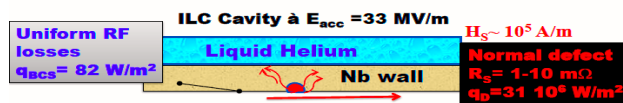


Figure 1: Sketch of the thermal model used (2D axisymmetric problem).

quadratic dependence of Joule RF losses with B_S (e.g. $q \propto R_S B_S^2$), the temperature of the RF surface T_{RF} increases strongly with B_S especially in the defect area. As illustration of such strong heating $\Delta T = T_{RF} - T_0$, the computed temperature profile is presented in Fig.2 for a field jute above the quench field.

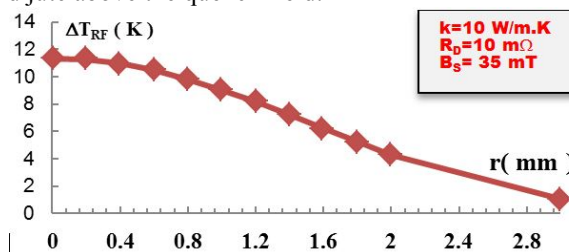


Figure 2: Computed heating profile (ΔT versus distance r to defect center) on the RF surface (Bath Temperature: $T_0=2$ K, defect radius: 200 μm , $E_{acc}=9$ MV/m).

As E_{acc} is increased, The Joule heating increases the RF surface temperature (Fig. 3) in the vicinity of the defect up to the critical temperature T_C (B_S) of niobium. When the quench field is reached, a dramatic increase (e.g. by 5 to 6 orders of magnitude) of the local RF losses is observed.

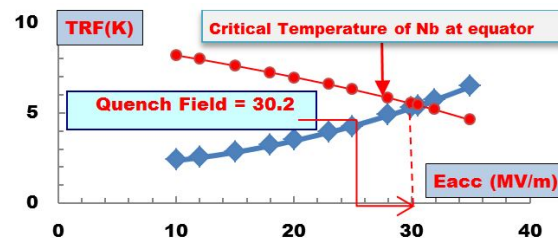


Figure 3: Computation of quench field for ILC cavity.

This catastrophic process leads to the quench of the SRF cavity as soon as the hot spot area effective diameter exceeds a critical value $D_C \sim 1-10$ cm, for which the unloaded quality factor Q_0 decreases strongly. Obviously, the thermal quench of a SRF cavity is easily detectable with RF probes (i.e. transmitted or reflected RF power). However, as it is an overall measurement, RF signals are insufficient to characterize completely the thermal runaway and are unable to locate quench source. Dedicated diagnostic tools are then needed in order to study and investigate in details quench phenomena.

BRIEF HISTORY OF DIAGNOSTIC TOOLS OF ANOMALOUS RF LOSSES IN SRF CAVITIES

The first generation of sensors to diagnose anomalous RF losses and thermal breakdown events was developed in ~1980. These sensors [2-4] are either Fixed Surface Thermometers (FST) or Scanning Surface Thermometers (SST), which measure the outer surface temperature the cavity cooled by Liquid Helium (LHe). To summarize [2-3] SST are intrinsically limited in superfluid helium or He II (low efficiency, lack of reliability/repeatability). The main drawbacks or limitation of FST is the need of a large number (i.e. $\gg 100$) of such sensors [3-5] in order to ensure a good spatial resolution. Second generation of quench detectors in He II, namely OST (Oscillating Super-leak Transducer), were developed in 1970 for fundamental studies of He II hydrodynamics [6]. The OST are capacitive quench detectors (QD), sensing second sound events in He II and were applied to SRF cavity thermal breakdown studies 7 years ago [7]. Note that Low Response Time ($\ll 1$ ms) resistive Thermometers (LRTTH) could also be used as quench detectors.

EXPERIMENTAL SET-UP

Description of OST Developed at IPN Orsay

The first generation of OST with 31.5 mm O.D was developed at IPN Orsay [8] was similar to that used at Cornell. A second generation of smaller OST have been developed at IPNO. The main features of these new OST are the following: 1) smaller footprint (O.D:13 mm), better mechanical precision resulting in a higher spatial resolution, 2) nearly unchanged sensitivity, 3) a better reliability and repeatability.

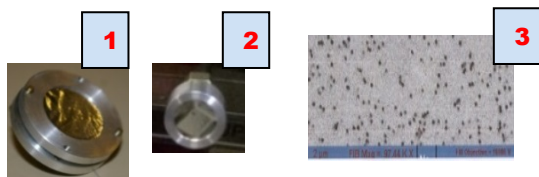


Figure 4: Photographs of first (1), second generation (2) of OST and SEM image (3) of the membrane.

Test Cells and Configuration of Sensors

The quench of SRF cavities is experimentally simulated by means of Joule heated resistors. A first test facility was previously used [8] for the calibration and full characterization of QD in the bath temperature (T_0) range 1.55 K– 4.25K. In order to improve the measurement sensitivity, the signal to noise ratio especially for thermometric signals, and mechanical precision for QD positioning, the facility was upgraded. More precisely, we used a more sophisticated PCB for heating sources and we improved wiring and shielding of thermometric signal

as well as mechanical support of quench detectors. In order to investigate the effect of the heater geometry, and the distance of the sensors to the quench-like source, we performed experimental runs with different configurations (6 test cells) using either cylindrical or flat SMD resistors of different sizes. Moreover, we used bare ship CERNOX resistors, named CX here after as LRTTH or QD. A photograph of the six new test cells (e.g. assembly of heaters, OST and CX sensors) used is shown in Fig. 5.



Figure 5: Test Cells and Configuration of Sensors.

Six different experimental configurations were tested, but only the results obtained with the test-cells #1 and #2 (see detailed description in Table 1) will be presented in this paper.

Table 1: Description and configuration of two out of six test-cells used

Cell #	Sensor	Configuration	Heater #1	Heater #2	Heater #3	Type
1			SMD 2.5	Cyl. 227.8	SMD 4.8	Type $A(\text{mm}^2)$
	OST7	Shielded	60.8	51.5	58	r (mm)
	OST8	unshielded	35.7	32.5	41.5	r (mm)
2			SMD 2.5	Cyl. 50.9	Cyl. 227.8	Type $A(\text{mm}^2)$
	CX1	Shielded	20.4	14	13	r (mm)
	CX2	unshielded	35.8	37	34	r (mm)

CHARACTERIZATION RESULTS AND TESTS ON CAVITIES

Experimental Procedure

Several experimental runs were performed at different T_0 . Prior to the measurements of the response of the QD (OST and CX) to a pulsed heat flux to which heaters are subjected, we calibrated (e.g. Resistance vs. T_0) the CX resistors by comparison to a reference thermometer. This calibration was performed in the LHe saturated bath (thermostat): a precise pressure transducer with a PID vapour pressure controller and a motorized butterfly valve allows the regulation of T_0 to within ± 0.2 mK for $T_0 < T_i = 2.1768$ K.

Response of Cernox Sensors at $T_0 = 1.9$ K

Using the SMD heater #1 (heater area: 2.5 mm^2) of the cell #2, we measured (Fig. 6) at $T_{\text{bath}} = 1.9$ K, the response of CX1 and CX2 to a pulsed heat flux applied to the heater (Peak value: 15.2 MW/m^2 , pulse duration: $\tau_p = 100$

μ s). It should be stressed that the measurement of such fast transient thermometric signals with a small heater (e.g. 2.5 mm²) in a large He II bath (ID: 350 mm, Height: 100 mm-750 mm) is challenging. For a baseline signals \sim 100 mV, we achieved a resolution better than 2 μ V at 100 kHz sampling rate. Moreover, for a sensing current of 20 μ A, the measured peak values are \sim 100 μ V leading to a peak transient heating \sim 100 μ K.

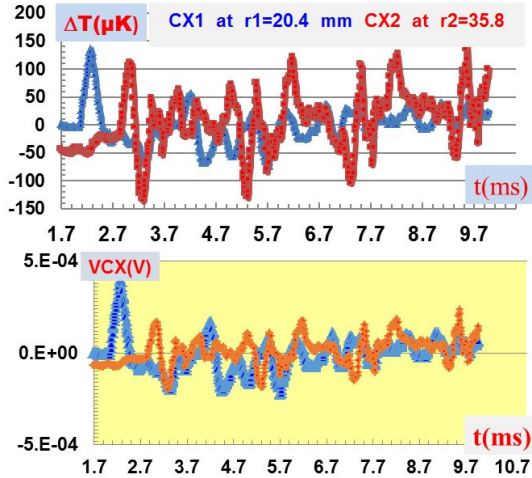


Figure 6: Response of CX1 and CX2 (Heater #, pulsed heat flux (Peak value: 15.2 MW/m², pulse duration: τ_p =100 μ s).

Further, from the observed time of flight $\Delta t=770 \mu$ s between the first peaks of the 2 sensors CX1 and CX2, we deduced a second sound velocity, measured by a pulse method, $u_2=20$ m/s at $T_0=1.9$ K: this value is close (6.1%) to reported by Donnelly [9] team (e.g. $u_2=18.77$ m/s) using resonant method (e.g. frequency measurement of 2nd sound resonator).

Second Sound Velocity

Using both OST and CX signals, we performed systematic measurements of the 2nd sound velocity from T_i down to 1.67 K. A cross-correlation method was applied for processing QD signal leading to the experimental variations of u_2 as function of T shown in Fig. 7. These measurements were performed using two different procedure: 1) stabilize T_0 at different values then subject heater to a pulsed heat flux and simultaneously monitoring OST and CX signals versus time, b) subject the heater to a fixed pulsed heat flux and simultaneously monitoring OST and CX signals versus time while T_0 is slowly drifting. Again our experimental data are in very good agreement with experimental results previously reported in the literature [9].

Response of OST Sensors to Pulsed Heat Flux

Using the heater #1 (area: 2.5mm²) of cell#1, we studied at $T_0=1.9$ K, the response (Fig. 8) of OST#8 and OST #7 at fixed $\tau_p=100 \mu$ s.

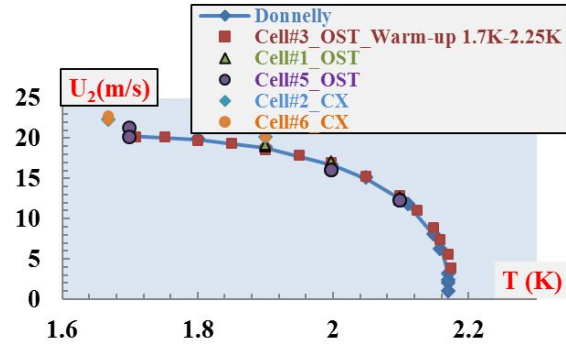


Figure 7: Comparison of measured second sound velocity to previous experimental data (solid blue line).

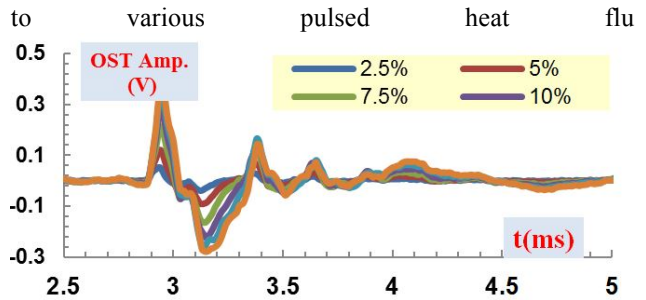


Figure 8: Effect of peak heat flux on OST response at $T_0=1.9$ K.

The data of Fig. 8 clearly show a linear dependence of peak amplitude as function of the peak heat flux (Fig.9). These results were observed for the two OST located respectively at a distance $r=35.7$ mm and $r=60.8$ mm.

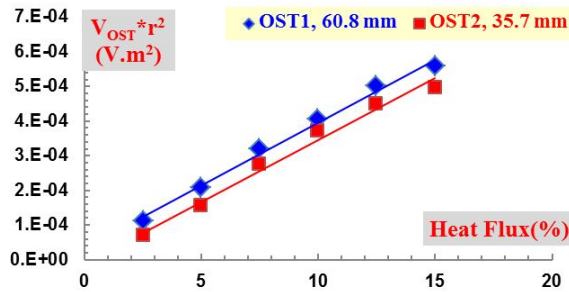


Figure 9: Effect of heat flux and distance to the heater on the response of OST#7 and #8.

For the SMD resistors (e.g. heaters configuration corresponding to a spherical symmetry), one expects a quadratic decrease of the heat flux with r (e.g. $q \propto r^{-2}$) as it is clearly observed in Fig. 9.

Quench Detection on Cavities

Several systematic tests were performed on 2 types of cavities developed by IPNO: 1) QWR operating at 88MHz for SPIRAL2, 2) Double-Spoke cavities for ESS project (Fig. 10). The design values of the Double-Spoke are: $f_0=352$ MHz, $E_{acc}=9$ MV/m ($B_{pk}= 61$ mT) and unloaded quality factor $Q_0=1.510^9$ at 2 K.

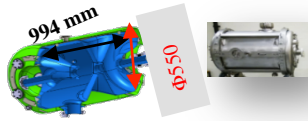


Figure 10: 3D drawing and photograph of ESS cavity Romea.

The achieved RF performances at $T=2K$ of the prototype cavity shown in Fig. 10 were beyond design values: $E_{acc} > 11.5$ MV/m and $Q_0 = 3.310^9$ at 9 MV/m. Due to the tight available space between the cavity and the LHe tank, only 2 OST were used and we successfully located the quench. More precisely, data analysis leads to 2 possible quench locations in one of the spokes: 1) in the spoke #1 (blue arrow in Fig. 11) at ~ 10 cm from the external wall of the cavity, 2) on the rim of spoke #2 (red arrow in Fig. 11). This result is statistically expected because the spoke are high surface magnetic areas (red regions in Fig. 12).

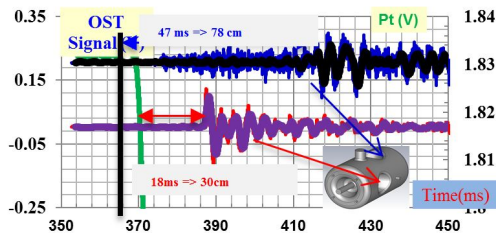


Figure 11: Detection and location of a quench in a Double-spoke cavity.



Figure 12: Surface magnetic field distribution (isovalues) in the fundamental mode.

SECOND SOUND RESONATOR

Description of the Second Sound Resonator

In order to perform precise measurements of the 2nd sound velocity u_2 in He II, we developed a Second Sound Resonator (SSR). This SSR (Fig. 13-Fig. 14) is equipped with a pair of OST at its 2 extremities as thermal source (OST#1) and sensor (OST#2), and a low thermal capacity heater with 2 thermometers CX#1 and CX#2. This SSR could be operated in the standard standing wave mode or in pulsed mode (i.e. thermal shock waves). Further 2nd sound could be either thermally generated (e.g. Joule heating) or via the normal fluid flow induced by the motion the OST#1 membrane (e.g. mechanic-heat effect). Conversely, 2nd sound could be detected either with the thermometer or with OST#2.



Figure 13: Photograph of 2nd sound resonator.

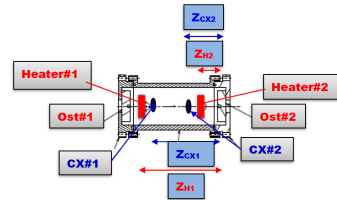


Figure 14: Diagram 2nd sound resonator instrumentation.

Description of SSR Tests

After the room temperature preliminary tests of the SSR as 1st sound resonator in gaseous helium, we performed experimental runs in liquid helium (i.e. first sound in normal and second sound in superfluid helium). These measurements were performed in two different operating conditions: 1) the SSR was operated in resonating mode (e.g. standing waves) with an AC excitation using a lock-in amplifier; 2) the SSR was operated in thermal shock wave mode and subjected to pulsed heat flux. The instrumentation block diagram is sketched in Fig. 15 in the case of AC excitation of 2nd sound.

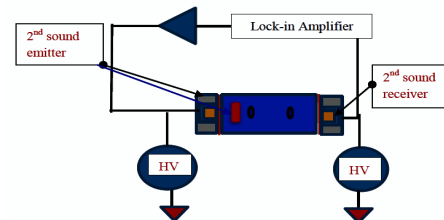


Figure 15: Block diagram of the instrumentation used for testing

First Sound Spectrum in Lhe at $T_0=4.2 K$

The measured and computed spectra (Fig. 16) are in very good agreement: more than 11 resonating mode were compared and the relative difference between measured and calculation results was less than 4.5 %.

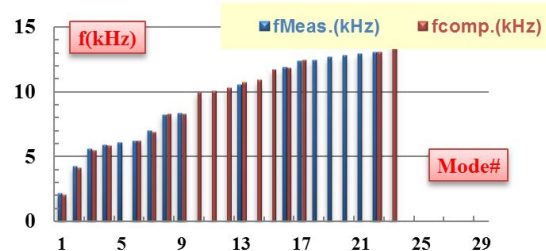


Figure 16: Measured and computed first sound spectra at $T=4.2 K$.

Furthermore, the quality factor $Q_1(n)$ of the 1st sound in Lhe at 4.2 K increases linearly with the mode number n : $Q_1(n) = 26.4n + 106$.

Second Sound Spectra in He II

The measured 2nd sound spectra at $T_0 = 1.7$ K, 1.9 K and 2.1 K are presented in Fig. 17. As expected, the data show an increase of the resonant frequencies f_{pmn} for all the modes when T is lowered. Obviously, this is attributed to the temperature dependency of 2nd sound velocity u_2 (e.g $f \propto u_2$). More precisely, the resonance frequencies of the different modes of the cylindrical SSR are given by:

$$f_{pmn} = \frac{1}{2} u_2 \left[\left(\frac{p}{L_R} \right)^2 + \left(\frac{a_{mn}}{R} \right)^2 \right]^{1/2} \quad (1)$$

Where the integer p is the mode number, L_R and R respectively, the length and the radius of the resonator. The parameter a_{mn} is the n^{th} root of the equation:

$$\frac{d[J_m(\pi.a)]}{da} = 0 \quad (2)$$

With J_m : Bessel functions of the first kind of order m .

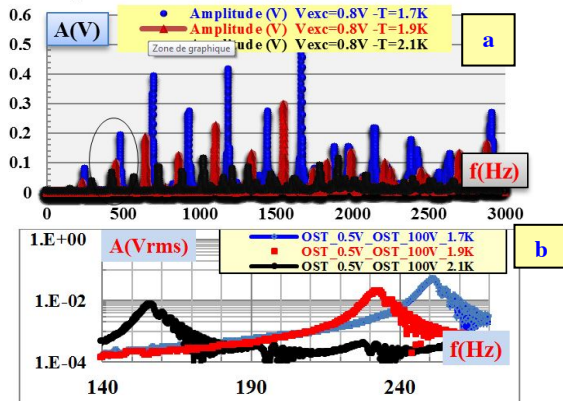


Figure 17: Effect of temperature on the measured second sound spectra in He II at $T = 1.7$ K, 1.9 K and 2.1 K.

Furthermore, 2nd sound spectra were measured (Fig. 18- Fig. 19) in four different configurations concerning wave generation (OST or Heater) and detection (OST or Cernox).

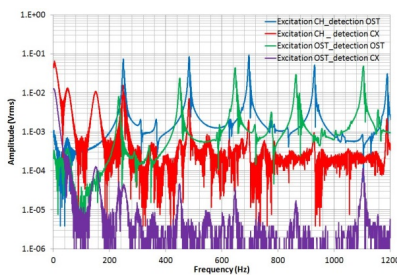


Figure 18: Comparison of 2nd sound spectra measured at $T_0 = 1.9$ K in four different configurations.

The tests of SSR were successful in the four above mentioned configurations leading to consistent experimental data which are in very good agreement with each other. For example, in the case where the OST#2 is used as 2nd sound detector, the measured frequencies of

the first mode are respectively $f_{1OST} = 233.6$ Hz (OST#1 as emitter) and 250 Hz.

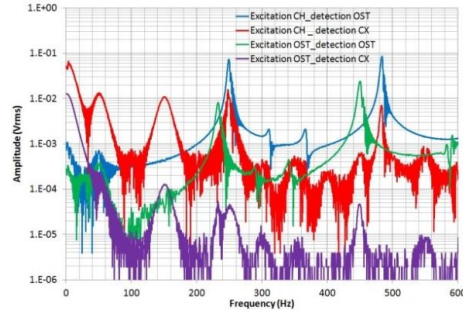


Figure 19: Comparison (zoom on first modes) of 2nd sound spectra measured at $T_0 = 1.9$ K in 4 different configurations.

The resulting ratio $b = 233.6/250 = 0.934$ is close to the expected theoretical value $b = L_{CH}/L_{OST} = 0.927$ where L_{CH} and L_{OST} are respectively the distances between the pair of 2nd sound emitter and receiver in each configuration.

ACKNOWLEDGMENT

Many thanks to all the technical staff of Accelerators Division and Instrumentation Division of IPN Orsay involved in the preparation of the experiments for their valuable help during all the tests.

REFERENCES

- [1] Y. Yamamoto et al., NIM A729 (2013) 589.
- [2] R. Brizzi, M. Fouaidy, T. Junquera, M.X. François "Thermometry of niobium surfaces in superfluid helium: a powerful diagnostic technique for superconducting RF cavities", HTD-Vol. 134, pp. 15-22, 1990.
- [3] M. Fouaidy et al., "Surface temperature measurements on superconducting cavities in superfluid helium" Proc. of SRF 1991, Hamburg, August 91, Vol. 2, pp 547 – 576.
- [4] M. Fouaidy et al., "Analysis of effects in TESLA SRF cavities using surface scanning thermometers", Proc. of EPAC96, Barcelona, June 96.
- [5] M. Fouaidy, T. Junquera, "Heat transfer characteristics from a plane surface to a saturated He II bath", Cryogenics Vol. 37, N° 11, pp. 753-765, 1997.
- [6] R. A. Sherlock and D. O. Edwards, "Oscillating Super leak Second Sound Transducers", The Review of Scientific Instruments Vol. 41, 11 (1970) 1603.
- [7] Z.A. Conway et al., TTC report #2008-06. [11]
- [8] M. Fouaidy et al., "Calibration and characterization of capacitive ost quench detectors for SRF cavities at IPN Orsay", Proc. of SRF2013, Paris, France, pp.714-718
- [9] R. T. Wang, W.T. Wagner, R. J. Donnelly, "Precision Second-Sound Velocity Measurements in Helium II", J. L.T.P, Vol. 68, Nos.5/6 (1987) 409.